NRC Research Press

NOTE

Water retention characteristics of iron ore fines

Hailong Wang, Junichi Koseki, and Tomoyoshi Nishimura

Abstract: Evaluations of water retention characteristics of typical iron ore fines (IOF) were presented, which was part of experimental works for the estimation of liquefaction potential of IOF heaps. The water retention tests were conducted in a suction range from 0.1 to 10^6 kPa on two IOFs and two artificial soils with various testing techniques. It is observed that water retention characteristic curves of one IOF (IOF-B) converge in terms of the relationship between suction (S) and water content (w) regardless densities of specimens when S exceeds a threshold value (S_{th}). Based on this finding, water retention characteristics are divided into density and materials affected zones. It is also found that IOFs generally have higher water retention ability than the two artificial soils, from which discussion is made on the effect of specific surface area and mineralogy on water retention characteristics of IOF. Finally, water retention characteristics are linked to compaction curves, from which, with the consideration that degree of saturation at peaks of compaction curves is relatively constant, a safety margin of a recently proposed regulation for maritime transportation of IOF is discussed.

Key words: iron ore fines, water retention characteristics, suction–volumetric water ratio relationship, compaction.

Résumé : Des évaluations de caractéristiques de rétention d'eau de fines de minerai de fer (« IOF ») typiques ont été présentées, ce qui faisait partie des travaux expérimentaux d'estimation du potentiel de liquéfaction de tas d'IOF. Les essais de rétention d'eau ont été réalisés dans une gamme de succion de 0,1 à 10^6 kPa sur deux IOF et deux sols artificiels en utilisant différentes techniques d'essais. On observe que les courbes de caractéristiques de rétention d'eau d'un IOF (IOF-B) convergent en termes de relation entre la succion (S) et la teneur en eau (w) indépendamment des densités des échantillons lorsque S dépasse une valeur seuil (S_{th}). Sur la base de ces résultats, les caractéristiques de rétention d'eau sont divisées en zones affectées par la densité et les matériaux. On constate également que les IOF ont généralement une capacité de rétention d'eau supérieure à celle des deux sols artificiels, d'où il est question de l'effet de la surface spécifique et de la minéralogie sur les caractéristiques de rétention d'eau de l'IOF. Enfin, les caractéristiques de rétention d'eau sont liées aux courbes de compactage, à partir desquelles, compte tenu du fait que le degré de saturation aux pointes des courbes de compactage est relativement constant, une marge de sécurité d'un règlement récemment proposé pour le transport maritime des IOF est examinée. [Traduit par la Rédaction]

Mots-clés : fines de minerai de fer, caractéristiques de rétention d'eau, rapport succion–humidité volumique, compactage.

Introduction

Iron ore fines (IOF) is a type of bulk cargoes commonly transported at sea. In 2009, casualties of two vessels loaded IOF happened near Indian ports (IMO 2010*a*, 2010*b*). These casualties were reportedly caused by liquefaction of IOF due to its high water content when being loaded to the vessels in the monsoon season. Some other bulk cargoes also seemed risky in terms of resisting liquefaction during maritime transportation (Roberts et al. 2013; Chen et al. 2014). As a regulation instruction of transporting solid bulk cargoes at sea including the aforementioned cargoes, the International Maritime Solid Bulk Cargoes (IMSBC) Code (IMO 2012) provides individual instructions for some specific cargoes (the individual instruction is called "individual schedule" in the code, and the term individual schedule can be regarded as a "check list of precautions" for transportation of a cargo). For cargoes that may liquefy, their transportable moisture limits (TML) are required to be determined using three optional methods before loading, and cargoes should not be allowed to be loaded when their water content exceeds TML. Unfortunately, there was not an individual schedule for IOF before the two casualties and some shippers followed another individual schedule named "Iron Ore" which was for iron ore with particle size up to 250 mm and treated as unliquefiable cargo (IMO 2010*b*, 2012).

According to the aforementioned background, a series of studies was conducted by an iron ore technical working group (TWG) under the supervision of International Maritime Organization (IMO) to build an individual schedule for IOF (IMO 2013*b*, 2013*c*, 2013*d*, 2013*e*, 2013*f*, 2013*g*). TWG conducted studies from mainly three aspects: (*i*) a marine study to identify and quantify the inertial forces that vessels and their cargoes experienced during ocean voyages (IMO 2013*d*); (*ii*) literature reviews, in situ and laboratory tests to develop a new test method, the modified Proctor–Fagerberg test (MPFT) for determination of TML of IOF (IMO 2013*e*); (*iii*) laboratory elemental and model tests and numerical simulations for validation of TML determined by MPFT in prevention of IOF liquefaction (IMO 2013*f*). Based on these studies, an individual schedule for "Iron Ore Fine" cargo was proposed, which has been applied mandatorily since 1 January 2017 to iron ore cargoes contains both (*i*) 10% or more of fine particles less than 1 mm and (*ii*) 50% or more of particles less than 10 mm (IMO 2013*a*, 2015).

Received 27 November 2018. Accepted 23 November 2019.

H. Wang. Waseda Research Institute for Science and Engineering, Waseda University, Tokyo, Japan; formerly Institute of Industrial Science, The University of Tokyo, Japan.
J. Koseki. Department of Civil Engineering, The University of Tokyo, Japan.
T. Nishimura. Division of Architecture and Civil Engineering, Ashikaga University, Japan.
Corresponding author: Hailong Wang (email: whlxy2002@gmail.com).

Fig. 1. Schematic illustration of method to determine transportable moisture limits (TML). MPFT, modified Proctor–Fagerberg test.

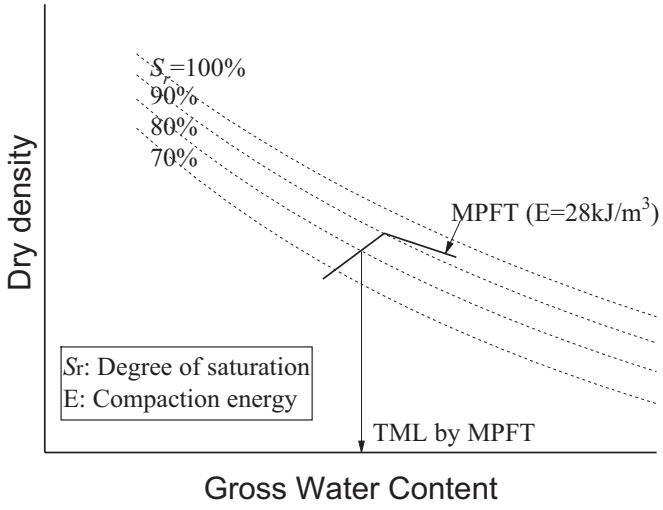

Fig. 2. Illustration of seepage process and its relation with liquefaction of iron ore fines (IOF) heap: (*a*) formation of saturated and unsaturated zones in heap due to seepage process; (*b*) cyclic shear stress development due to rolling motion of vessel at T2. [Colour online.]

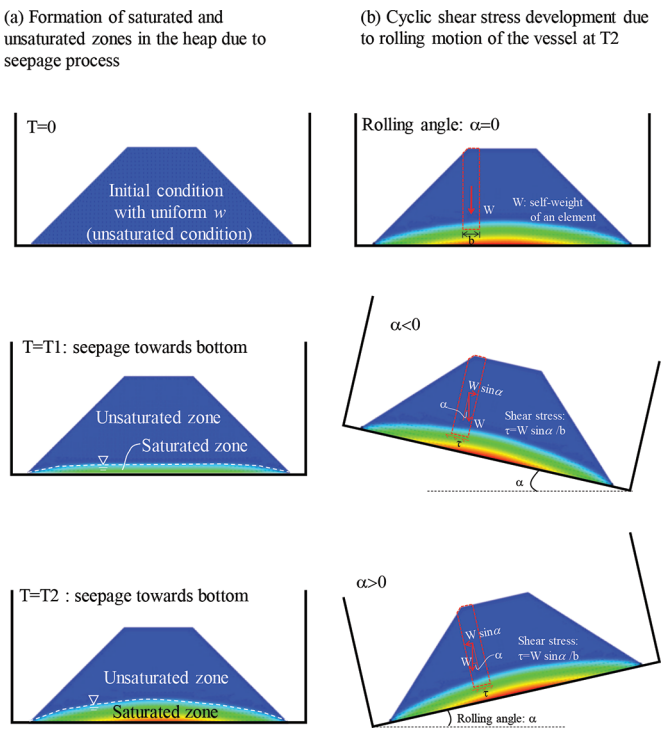

The MPFT, as the only method to determine TML of IOF, is essentially the same as the Proctor test, but with smaller compaction energy. And TML is assigned to be the gross water content (= mass of water/(mass of IOF + mass of water)) corresponding to the intersection of the compaction curve and 80% degree of saturation (S_r) line as shown in Fig. 1. It is worth mentioning that the term "gross water content" is commonly used in the industry of maritime transportation, though the gravimetric water content (w = mass of water/mass of solid) is mainly used for discussion in this paper except for specific clarification. TWG suggested the liquefaction of IOF with S_r less than 80% would not happen according to observations in triaxial tests of TWG reports. Notwithstanding such a finding, with utilization of a newly developed triaxial system (Wang et al. 2016*c*, 2017*b*, 2017*c*), Wang et al. (2016*a*) revealed that IOF elements with S_r less than 80% may also liquefy. On the contrary, Fig. 2 schematically illustrates a mechanism of IOF heap liquefaction according to TWG reports (IMO 2013*f*). First a saturated zone probably forms by seepage of initially unsaturated IOF (Fig. 2*a*) and then liquefaction may develop due to a cyclic shear force induced by self-weight of IOF and rolling motion of the vessel (Fig. 2*b*). Wang et al. (2017*a*) conducted preliminary numerical simulations to evaluate the liquefaction potential of an IOF heap based on their laboratory test results (Wang et al. 2014, 2016*a*, 2016*b*, 2018) and pointed out that not only the saturated zone, but the unsaturated zone of IOF heap may also have high liquefaction potential.

Fig. 3. Typical conditions of heaps of IOF. *D*, diameter; *H*, height. [Colour online.]

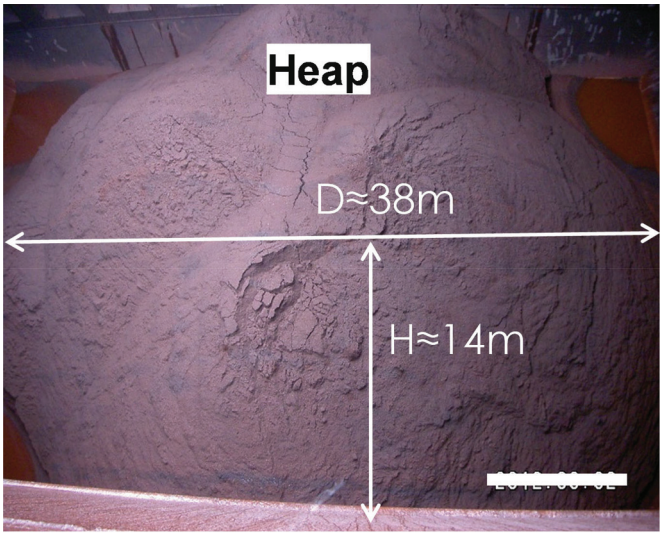

The first step in estimations of liquefaction potential of an IOF heap is to know w or S_r distribution of the heap through in situ investigations, seepage analyses, etc. The authors involved in some inspections on the shipped IOF, according to the in situ conditions as shown typically in Fig. 3, determined that in situ investigations would be difficult and costly. In the case of seepage analyses, permeability of IOF under different conditions (e.g., S_r and density) is preferable. Wang et al. (2019) and Tan Tian (2019) conducted some permeability tests for unsaturated IOF; however, test results

Table 1. Properties of materials tested in this study.

Material	D_{max} (mm)	F_c (%)	G_s	Density or material composition information	Classification by USCS (ASTM 2003*a*)
IOF-A	19	17.8	4.835	—	Silty sand with gravel
Ref-A	19	17.9	2.694	C:N:DL = 75.3%:11.5%:13.2%	
IOF-B	9.5	23.6	4.444	ρ_{dmax} = 2.79 Mg/m^3, w_{opt} = 12.0%	Silty sand
Ref-B	9.5	23.6	2.678	C′:N:DL = 50.9%:33.1%:16.0%	

Note: D_{max}, maximum particle size; F_c, percentage of particles less than 0.075 mm by weight; G_s, specific gravity; ρ_{dmax} and w_{opt}, maximum dry density and optimum water content obtained by standard Proctor compaction test, respectively; C, C gravel; N, N sand; DL, DL clay; C′, C gravel after removing particles over 9.5 mm; C:N:DL and C′:N:DL, percentages of each materials by weight in Ref-A and Ref-B, respectively.

were limited, and it is difficult to estimate permeability of IOF with neither a full range of S_r nor different density conditions. Thus, in this study the water retention characteristics of IOF obtained from laboratory tests were presented as a part of testing works by the authors, in which the effect of density conditions on characteristics of water retention is discussed. Additionally, in the individual schedule for "IRON ORE FINE" cargo, the effect of a mineral component, goethite (α-FeO(OH)), in IOF was considered as an exemption condition in the judgement of liquefaction potential of IOF. Based on this study, comparisons between IOF and common geomaterials and discussions about effect of mineralogy in terms of water retention characteristics are also given.

Test materials

IOF is produced by crushing of iron ores for utilization in the iron–steel making industry. Iron ores can be regarded as natural rocks that are rich in iron oxides in the form of such a mineral as magnetite (Fe_3O_4), hematite (α-Fe_2O_3), goethite (α-FeO(OH)), limonite (FeO(OH)·n(H_2O)) or siderite ($FeCO_3$) (Ramanaidou and Wells 2014). Tests in this study were conducted on two typical IOFs (IOF-A and IOF-B) and their two reference materials (Ref-A and Ref-B), respectively, to obtain their water retention characteristics. Material properties related to this study are summarized in Table 1 and their gradation curves are shown in Fig. 4. Though mineral analyses could not be conducted, the major iron-rich minerals in IOF-A and IOF-B would be hematite and goethite, respectively, according to IMO (2013*f*) and personal communications with related traders and producers. The two reference materials were artificially mixed by using three soils (i.e., DL clay, N sand, and C gravel) in a way that reference materials and their corresponding IOFs had the same maximum particle size and percentages of passing 2 and 0.075 mm sieves. C gravel was a commercial product with maximum size of 19 mm, while to match gradation with IOF-B, particles larger than 9.5 mm were removed for Ref-B. Thus, the original gradation can be classified into well-graded gravel with sand and well-graded sand with gravel for gradation adjusted C gravel. N sand, which can be classified as silty sand, was obtained at a construction site and DL clay was also a commercial product classified as silt. The fines (particle size < 0.075 mm) both in IOFs and references were all nonplastic materials. Water retention characteristics of the reference materials herein were regarded as general representatives of common geomaterials.

Preparations and procedures for tests on water retention characteristics

Tests were conducted in three suction ranges as shown in Table 2 (i.e., 0.1–20 kPa, 0.1–100 kPa, and 10^3–10^6 kPa) to examine effects of void ratio (suction ranges: 0.1–20 kPa, IOF-B only) and material (suction ranges: 0.1–100 kPa and 10^3–10^6 kPa). Pressure plate and vapor equilibrium techniques were employed in different suction ranges. For the apparatuses using the pressure plate technique as shown in Fig. 5, the membrane filter and ceramic disk pedestals were employed for suction ranges of 0.1–20 kPa and 0.1–100 kPa, respectively. The air entry values (AEV) of the two pedestals were 250 kPa, while a maximum suction of 20 kPa was

Fig. 4. Gradations curves of materials used.

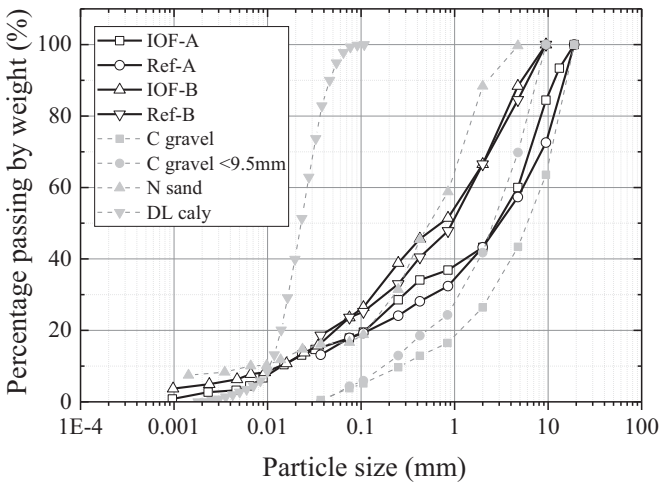

applied to the membrane filter pedestal to avoid air diffusion during tests. The thicknesses of the used ceramic disk and membrane filter were 4 and 0.14 mm, respectively (for more information on the membrane filter technique, see Nishimura et al. (2012) and Wang et al. (2017*c*)).

Specimens used in the pressure plate apparatus were constituted by means of static compression. Distilled water corresponding to a gravimetric water content (w) of 10% was mixed with materials before compression, and compressed specimens were of 60 mm in height and 50 mm in diameter for IOF-A and Ref-A, and of 20–25 mm in height and 50 mm in diameter for IOF-B and Ref-B. A higher dimension was chosen for IOF-A and Ref-A considering the maximum particle size of the two materials. Dimensions of specimens were determined based on experiences: Wang et al. (2017*c*) conducted repeat tests on IOF-B specimens with height of 20–26 mm and diameter of 50 mm, and obtained very consistent water retention curves, which also imply specimen dimensions in this study may be proper. However, as no experimental data are available for materials with larger particle size (i.e., IOF-A and Ref-A), further study may also be necessary to confirm the effect of specimen size on water retention characteristics. Specimens were, after being fixed to the pedestal and covered by the cap, saturated by soaking in a water tank and by applying a negative pressure near –100 kPa overnight. Thereafter, the elevation of the top of specimens was kept the same as the water level in the burette (refer to Fig. 5*a*) overnight for initial stabilization. Values of initial degree of saturation (S_{r0}) of specimens tested on pressure plate apparatuses as shown in Table 2 correspond to the state after initial stabilization, and S_{r0} > 100% condition for some specimens may be because some water stored in the top opening of the apparatus did not sufficiently flow out (refer to Fig. 5*b*). The drying process was executed by increasing suction step by step. Suction up to 20 kPa was applied by lifting the specimen up to a higher elevation than the water level in the burette, while a higher suction was applied by the axis-translation technique. The wetting

Table 2. Specimen conditions of tests for water retention characteristics.

Test method	Suction range (kPa)	Material	Test name	ρ_d (Mg/m^3)	S_{r0} (%)	e
Pressure plate apparatus with membrane filter pedestal	0.1–20	IOF-B	IOF-B_m1	2.01	100	1.214
			IOF-B_m2	2.45	104	0.814
			IOF-B_m3	2.57	103	0.727
			IOF-B_m4	2.73	103	0.629
Pressure plate apparatus with ceramic disk pedestal	0.1–100	IOF-A	IOF-A_c	2.96	76	0.636
		Ref-A	Ref-A_c	1.99	90	0.356
		IOF-B	IOF-B_c	1.97	108	1.260
		Ref-B	Ref-B_c	1.47	104	0.821
Vapor equilibrium technique	10^3–10^6	IOF-A	IOF-A_v	3.03* (3.02–3.05)	82	0.592
		Ref-A	Ref-A_v	2.01* (2.00–2.03)	80	0.336
		IOF-B	IOF-B_v	2.00* (1.97–2.02)	36	1.221
		Ref-B	Ref-B_v	1.45* (1.41–1.50)	32	0.841

Note: ρ_d, specimen's dry density; S_{r0}, initial degree of saturation before drying or wetting process; e, void ratio.
*These values were estimated by extra tests and values in parentheses are ranges as described in the text.

Fig. 5. Schematic drawing of testing apparatus for water retention characteristics: (*a*) measurement system by pressure plate apparatus; (*b*) details of pressure plate apparatus with ceramic disk pedestal; (*c*) details of membrane filter pedestal: other parts are same as (*a*). [Colour online.]

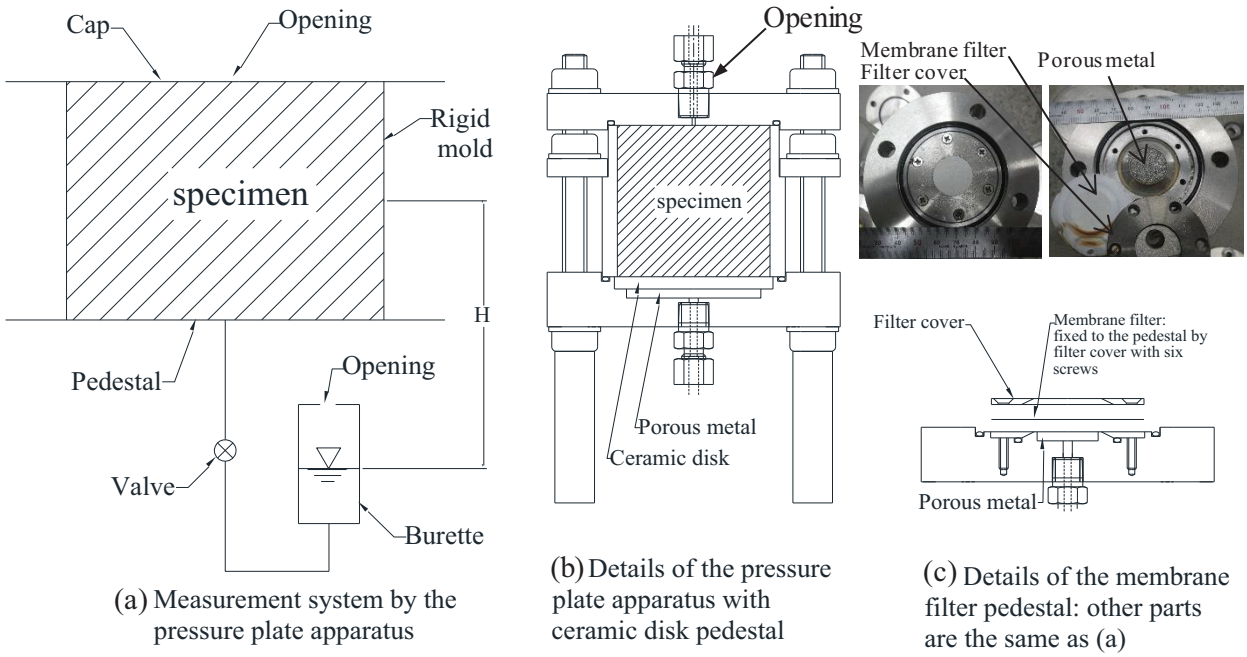

Fig. 6. Typical drainage time history for pressure plate apparatuses with (*a*) membrane filter pedestal; (*b*) ceramic disk pedestal. *e*, void ratio.

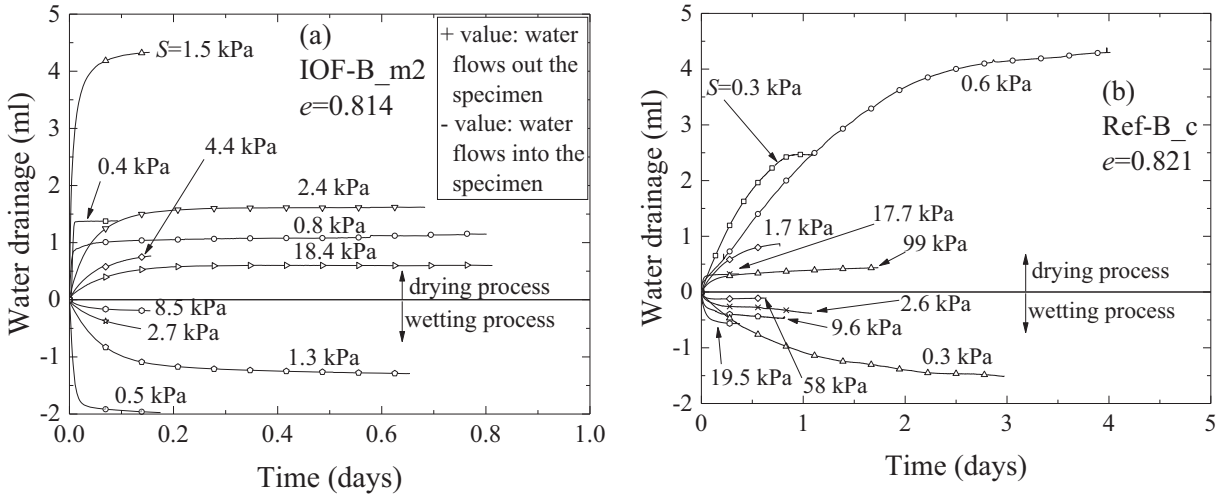

Fig. 7. Leak-proof chamber and specimen with vapor equilibrium technique: (*a*) specimen curing; (*b*) compaction; (*c*) IOF-A; (*d*) Ref-A; (*e*) IOF-B; (*f*) Ref-B; (*g*) density determination. [Colour online.]

Table 3. Chemical solutions and their corresponding relative humidity (RH) and total suctions.

Saturated chemical solution	K_2SO_4	KNO_3	$NH_4H_2PO_4$	NaCl	$Mg(NO_3)_2 \cdot 6\,H_2O$	$MgCl_2 \cdot 6\,H_2O$	LiCl
RH (%)	97.6	94.2	93.2	75.5	54.2	32.9	11.0
Total suction (MPa)	3.2	8.0	9.4	37.4	81.5	148.0	293.8

process was executed in a similar way following the last step of the drying process. Water content change of specimens was monitored by manual reading and a differential pressure transducer. Figures 6*a* and 6*b* illustrate typical water drainage time histories during application of suction (only typical suction steps are shown for visual convenience). It can be seen that water drainage equilibrium is reached much faster for the membrane filter pedestal compared to that of the ceramic disk pedestal. The possible volume changes of tested specimens while applying suction were ignored based on observations that there was no apparent volumetric change.

The vapor equilibrium technique is a common way to apply a total suction between 10^3 and 10^6 kPa. The principle of this method is to keep relative humidity (RH) of the environment surrounding specimens constant by chemical solutions, by which, depending on their total suctions, specimens either absorb water from or repel pore water to the environment until equilibrium. There are generally two components in total suction, matric suction (or capillary component of free energy) and osmotic suction (or solute component of free energy) (for more details, see for instance, Fredlund et al. (2012), Chap. 4). In this study seven chemical solutions were used to maintain specific RH in leak-proof chambers as shown in Fig. 7*a*. The specific RH values at the room temperature of this study (15.6 ± 1 °C) are shown in Table 3; they were determined based on Young (1967), Haynes (2010–2011), and JGS (2009) standard 0151. Furthermore, the applied total suction

Fig. 8. Typical time history of specimens in drying and wetting process with vapor equilibrium technique.

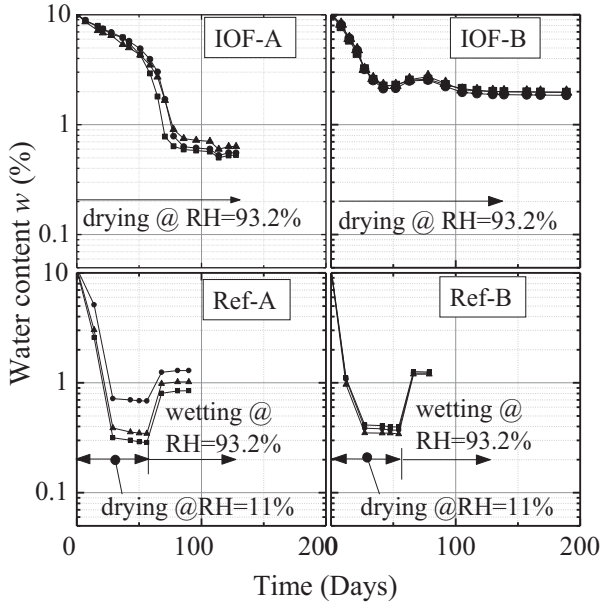

Fig. 9. Water retention curves of IOF-B specimens with different void ratios plotted with relationships of (*a*) suction–gravimetric water content; (*b*) suction–degree of saturation; (*c*) suction–volumetric water content.

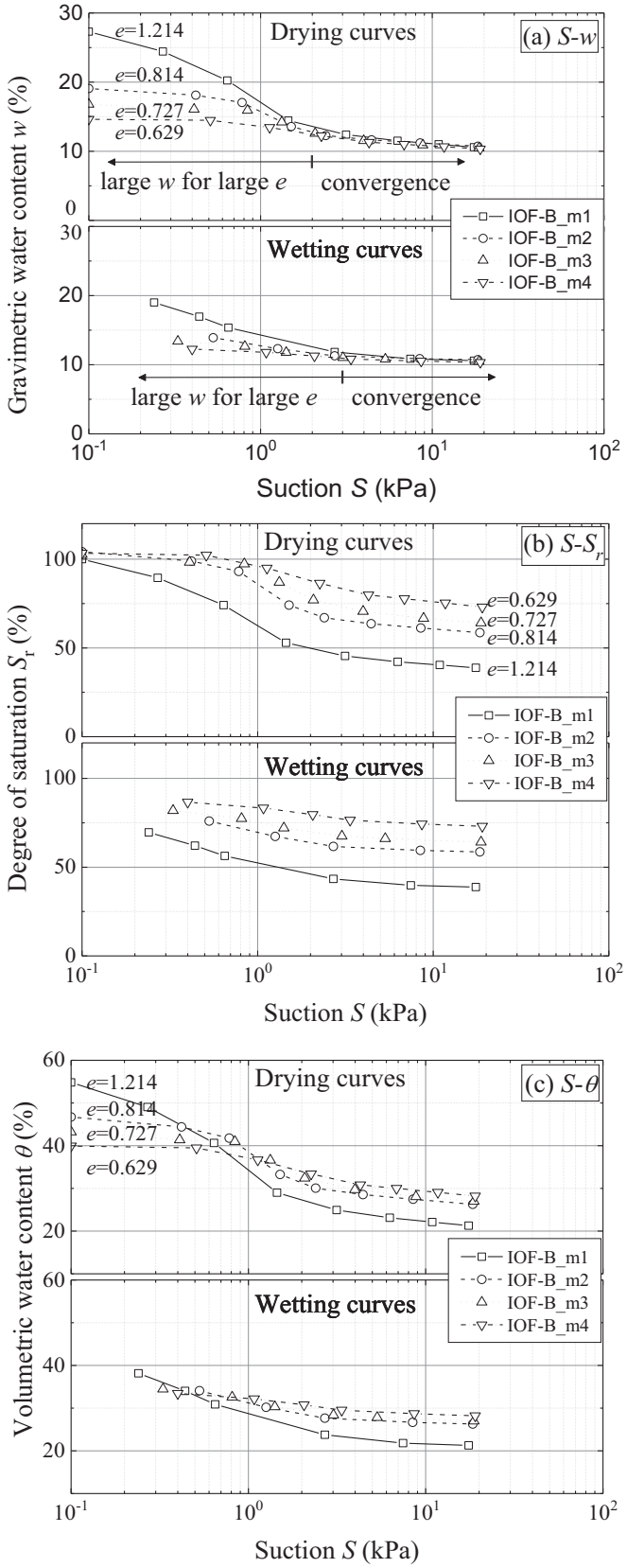

Fig. 10. Illustration of water retained by (*a*) individual particles; (*b*) voids between individual. [Colour online.]

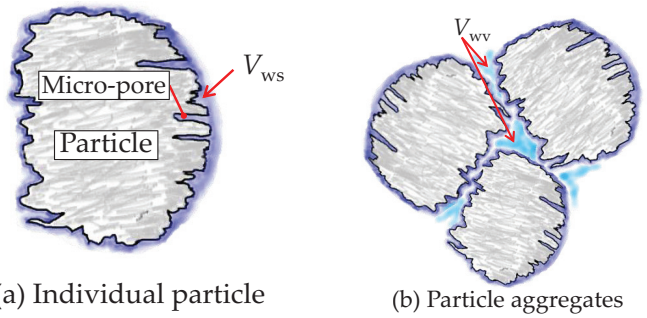

Fig. 11. Void ratio and material affected zones in R_w–S relationship for IOF-B: (*a*) drying process; (*b*) wetting process.

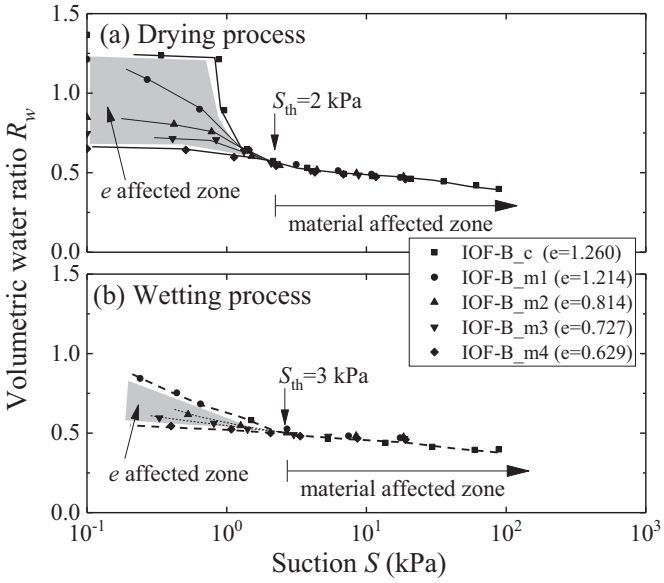

was calculated using RH (for the calculation equation, see, e.g., eq. 4.1 in Fredlund et al. 2012). The osmatic suction was estimated according to measured electric conductivity of solutions of tested materials following JGS (2009) standard 0151, which was less than 1 kPa for all tested materials and thus ignored herein ("suction" is used to denote matric suction in this study except for specific clarifications). Additionally, in the real condition, pore water inside IOF would be mostly freshwater (e.g., industrial water, rainwater) because sea water would not normally enter into IOF during either the crushing process, storage or maritime transportation. Thereafter, water used in this study was distilled water.

Specimens used for the suction range of 10^3–10^6 kPa were prepared in petri dishes by mixing oven dried materials with water (corresponding to w = 10%) and then compacted by free-fall of the petri dishes from a height of 10 mm 10 times. Water retention characteristic of tested materials were not expected to be affected by density conditions in such a large suction range; therefore, only small compaction energy was applied to make specimen surface even and to estimate density easily. The compaction condition is illustrated in Fig. 7*b* and for each specific RH, three identical specimens were prepared for each material for either the drying or wetting process. The typical conditions immediately after compaction are shown in Figs. 7*c*–7*f*. Water was apparent during the specimen preparation for IOF-A and Ref-A and less apparent for IOF-B and Ref-B. To estimate the dry density (ρ_d) of the prepared specimens, compaction testing was conducted in the

Table 4. Material properties and testing condition in past studies.

Reference	Soil name; USCS	LL; PI	G_s	e_0	w_0 (%)	S_{r0} (%)
Lins and Schanz (2005)	Hostun sand; SP	NP	2.65	0.89	~33.4	~99.5
				0.66	~24.5	~98.3
Gallage and Uchimura (2010)	Edosaki sand; SM	NP	2.75	1.254	~36.0	~79.0
				1.037	~30.4	~80.6
				0.883	~24.7	~76.9
	Chiba soil; SM	NA; 2.3	2.72	1.176	~42.3	~98.0
				1.015	~35.6	~95.5
				0.915	~31.8	~94.4
Huang et al. (1998)	Silty sand; SM	22.2; 5.6	2.68	0.525	~19.6	~100
				0.490	~18.3	~100
				0.474	~17.7	~100
				0.454	~16.9	~100
				0.426	~15.9	~100
Salager et al. (2010)	Clayey silty sand; SC–CL	25; 10.5	2.65	1.01	38.1	100.0
				0.86	32.3	99.5
				0.68	25.7	100.2
				0.55	21.0	101.2
				0.44	16.5	99.4
Gao and Sun (2017)	Pearl clay; CL	43; 17.5	2.71	1.32	45	92.4
				1.21	40.2	90.2
				1.09	37.6	93.1
Birle et al. (2008)	Lias–clay powder; CL	46.5; 27	2.78	0.497	15.5	86.7
				0.568	17.1	83.7
				0.66	22.4	94.4

Note: USCS, classification by Unified Soil Classification System (ASTM 2003*a*); SP, poorly graded sand; SM, silty sand; SC-CL, clayey sand with fines leaning to clay; CL, lean clay; LL, liquid limit; PI, plastic index; NA, data is not available; NP, nonplastic soil; e_0 and w_0, void ratio and water content before drying, respectively; "~", data calculated based on first point of their corresponding water retention curve.

same way in a metal cylindrical container with a constant volume as shown in Fig. 7*g*. This test was repeated at least three times for each material, and each average value and its range is shown in Table 2. For the wetting process, specimens were all first stored in the chamber with RH of 11.0% until equilibrium, then delivered to other chambers with higher RH. The equilibrium was determined based on mass change of three identical specimens with a tolerance of 1–2 mg between two successive measurements (about 2 weeks). The typical results are shown in Fig. 8, which indicates that the final w values of identical specimens are very close, thought the equilibrium process is generally time consuming.

Results and discussions

Void ratio effect on water retention characteristics of IOF-B

Water retention curves of IOF-B specimens with different void ratio (e) are plotted in terms of S–w, S–S_r, and S–θ relationships in Fig. 9, where S and θ stand for suction and volumetric water content, respectively. Note that the initial conditions of specimens before applying any measurable suction were also plotted in Fig. 9 by assigning S = 0.1 kPa. It can be seen from Fig. 9*a* that for either drying or wetting curves, w is larger for a specimen with a larger e when suction is less than 2–3 kPa, while S–w relationships seem to converge to a unique line when suction increases gradually. On the contrary, in terms of the S–S_r relationship (Fig. 9*b*) a higher S_r seems to correspond to a specimen with lower e except near full saturation. Furthermore in terms of the S–θ relationship (Fig. 9*c*), it seems that a specimen with higher e has a larger θ for relatively low S (i.e., S < ~0.5 kPa) and a lower θ for relatively high S (i.e., S > ~2 kPa).

S–S_r and S–θ relationships have been used extensively in the past; however, increasing evidence (Romero et al. 1999; Kawai et al. 2000; Gallage and Uchimura 2010; Salager et al. 2010; Gao and Sun 2017) shows that there is a unique S–w relationship for a material regardless of its e when S exceeds a certain value. This finding was interpreted by the bimodal distribution character of void in a specimen (Delage and Lefebvre 1984; Romero et al. 1999). It was stated that void could be divided into the interaggregate

Fig. 12. Classification of fine-grained fraction of soils according to USCS (ASTM 2003*a*).

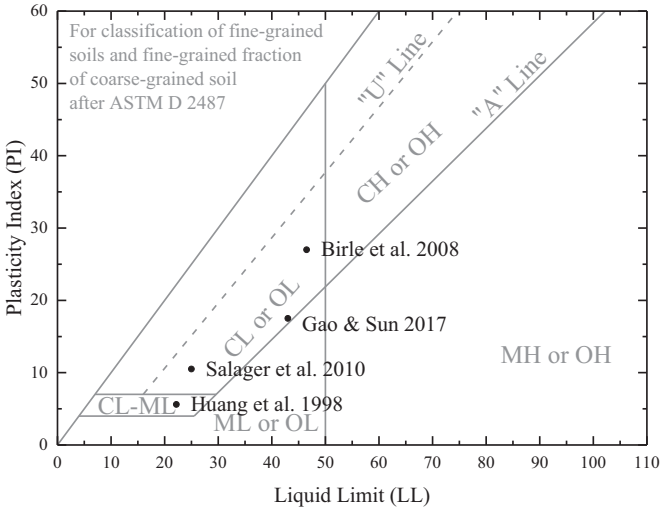

pores, which indicated pores between particle aggregates, and the intraaggregate pores, which denoted pores inside aggregates. The size of interaggregate pores is normally larger than that of intraaggregate pores suggesting that pore water is first exhausted from interaggregate pores under relatively small S and then from the intraaggregate pores under relatively large S in the drying process (similarly, intraaggregate pores first absorbed water for the wetting process). It was also shown that intraaggregate pores might not be affected significantly by compaction energy, and as a result w would be the same for specimens of a material with different e values when suction was high.

The preceding interpretation may be extended further to the individual particle level. For an individual soil particle as shown schematically in Fig. 10*a*, water can be retained in the micro pores

Fig. 13. R_w–S relationship for geomaterials obtained in past studies.

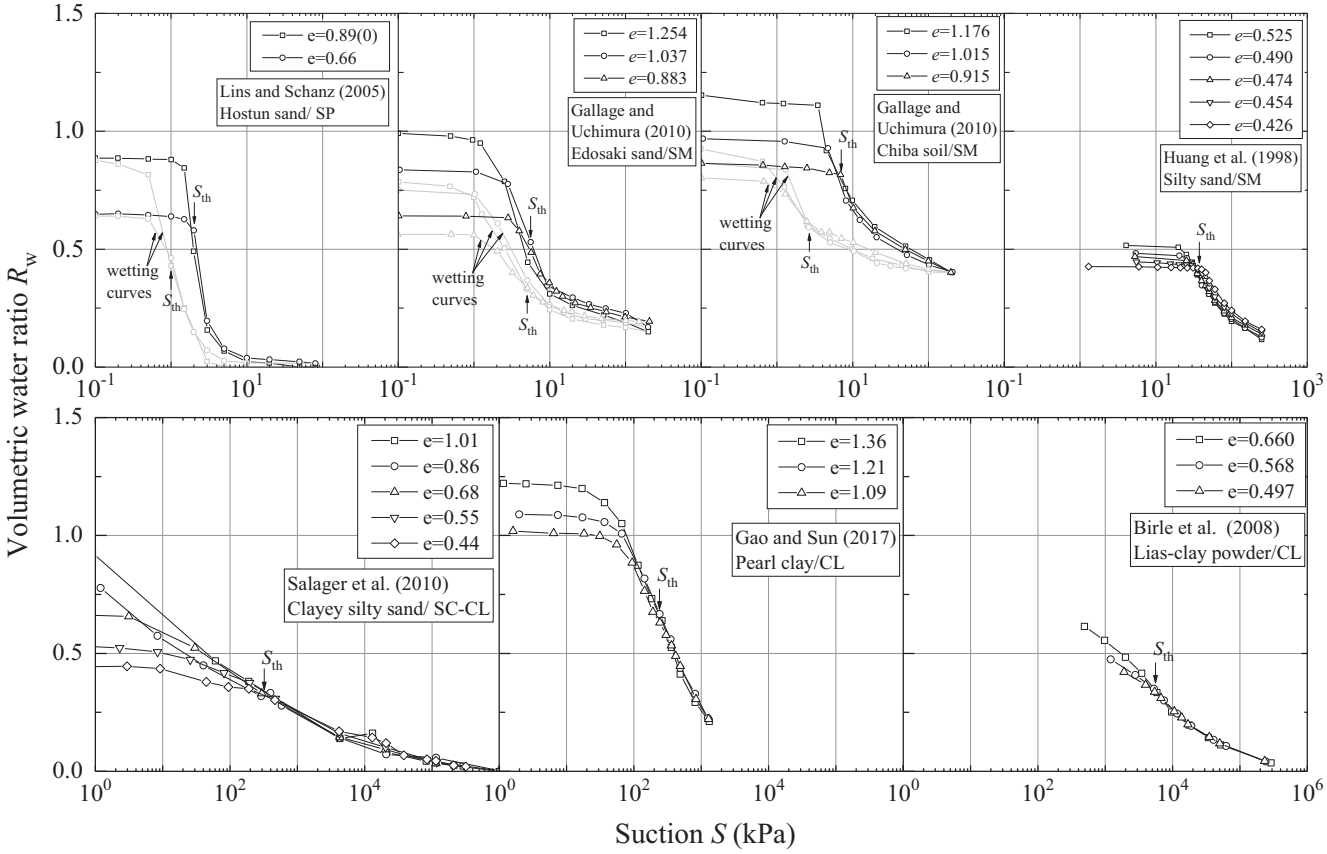

(i.e., concave surface) and on the convex surface. The volume of these water is named the intraparticle water (V_{ws}), which is a terminology often used in diffusion analysis inside the particles (Weber and Morris 1963; Higuchi et al. 2017). On the contrary, with the increase of the number of particles, water may be retained further in the voids. This water is named interparticle water (V_{wv}) as illustrated in Fig. 10*b*. V_{ws} and V_{wv} are all retained by the capillary force (i.e., matric suction); however, the capillary force is a net force of cohesion and adhesion forces, where the adhesive force is the attractive force between particle surface and water, and the cohesion force is the attractive force between water molecules. From the illustration of Fig. 10, it would be reasonable to regard that V_{ws} is mainly governed by the adhesion force (i.e., surface properties of solids), and V_{wv} is mainly governed by the cohesion force (i.e., void properties a solid mixture). Thus, it is assumed herein that V_{ws} is proportional to surface area of soil particles with a factor of t_w, then w can be expressed in eq. (1):

$$(1) \qquad w = \frac{1}{G_s}\frac{V_w}{V_s} = \frac{1}{G_s}\left(\frac{V_{wv}}{V_s} + \frac{V_{ws}}{V_s}\right) = \frac{1}{G_s}\left(\frac{V_{wv}}{V_s} + t_w \mathrm{SSA}\right)$$

where G_s is specific gravity; V_w is the total volume of water in the specimen; V_s is the volume of soil particles; $V_{ws} = t_w V_s \mathrm{SSA}$; t_w is a factor indicating an average thickness of the water film covering the particle surface by V_{ws}; SSA is the specific surface area (= total surface area of solid phase per unit of solid volume with units of m^2/m^3).

Equation (1) implies that w is not a function of e when $V_{wv} = 0$ and thus S–w relationships of specimens with different e can converge to a unique line. Indeed, eq. (1) is essentially the same as that of the aforementioned bimodal explanation if aggregates can be regarded as generalized individual particles. Additionally, if V_{ws} and V_{wv} can be separated, comparison of water retention ability between materials can be done by V_{ws} without considering e (i.e., V_{wv}) of specimens. With this purpose, a new parameter, volumetric water ratio (R_w) is defined in eq. (2):

$$(2) \qquad R_w = \frac{V_w}{V_s} = \frac{V_{wv}}{V_s} + \frac{V_{ws}}{V_s} = \frac{V_{wv}}{V_s} + t_w \mathrm{SSA}$$

Then it is assumed herein that water in V_{wv} always drains out first until it approaches 0 and then V_{ws} starts to drain as S increases in the drying process. Similarly, in the wetting process, water first goes to V_{ws} until maxima and then goes to V_{wv}. Under such an assumption, water retention curves in S–R_w space may be separated into V_{wv} and V_{ws} affected zones (i.e., e and material affected zones) as explained below.

S–R_w relationships of IOF-B conducted in this study are plotted in Fig. 11. It can be seen that S–R_w relationships converge when S exceeds a threshold value S_{th} (i.e., S_{th} = 2 kPa for the drying and 3 kPa for the wetting processes). The converged part may be regarded as V_{ws} affected zones or material affected zone, given that this part is not affected by e. On the contrary, the area between the lines of the loosest and densest specimens for $S < S_{th}$ as shown by the shaded areas may be regarded as V_{wv} or e affected zone. Because the AEV of a dense specimen would be larger than that of a loose specimen, other curves of initially saturated specimens with e values between e values of loosest and densest specimens are expected to appear in the shaded areas.

For other soils, Table 4 lists some results of past studies (Lins and Schanz 2005; Gallage and Uchimura 2010; Huang et al. 1998; Salager et al. 2010; Gao and Sun 2017; Birle et al. 2008) on both sandy and clayey soils, of which classification of fines in some soils are plotted in Fig. 12, and S–R_w relationships and their S_{th} of these

Fig. 14. S–R_w relationship of IOFs and reference materials (*a*) in suction range 0.1–100 kPa and (*b*) enlargement in range of 10^3–10^6 kPa.

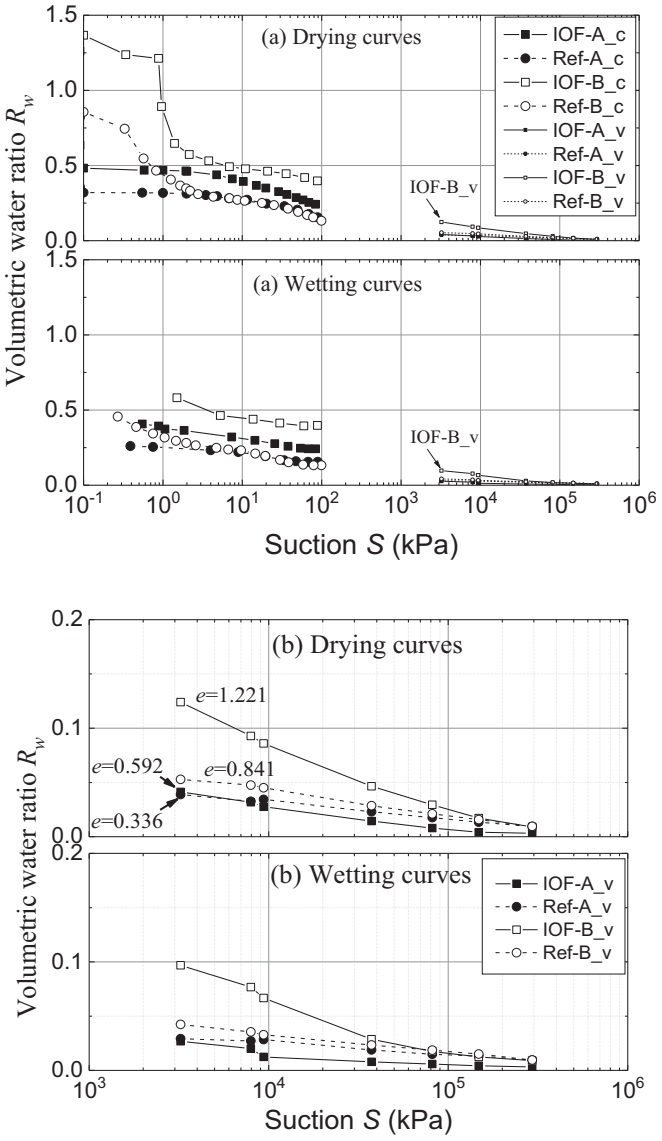

soils are shown in Fig. 13. It can be seen that for nonplastic sands, S_{th} is small (say <10 kPa), and there is a trend that S_{th} increases as plasticity index (PI) of soils increases.

Water retention characteristics of IOFs

S–R_w relationships of specimens conducted in the suction ranges of 0.1–100 kPa and 10^3–10^6 kPa are shown in Fig. 14*a* and an enlargement for suction range of 10^3–10^6 kPa is shown in Fig. 14*b*. It can be seen that R_w values of IOFs are larger than their corresponding reference for S < 100 kPa. And for $S > 10^3$ kPa, R_w values of IOF-B are still higher while those of other three materials become very similar both for drying and wetting curves. For Ref-A and Ref-B, it is shown that R_w values are very close when S > ~2 kPa in the drying process and when S > 4 kPa in the wetting process. Ref-A and Ref-B are mixtures of three common geomaterials with different content ratios, so they should be regarded as different materials, and the close result may be a coincidence. Additionally, though in this study water retention ability of IOFs seems to be larger than their references, it is lower compared to Chiba soil as shown in Fig. 13 implying that water retention ability of IOFs would not be significantly different from common soils.

Fig. 15. Characteristic of S–R_w and S–w relationships for IOF-B.

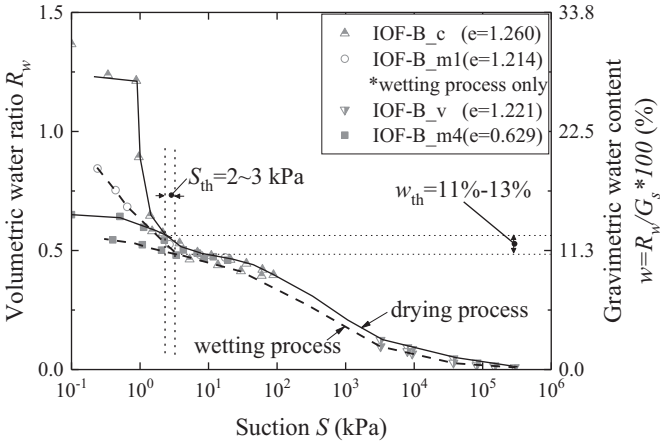

It is apparent that water retention ability of IOF-B seems to be stronger than that of IOF-A in the full suction range. One of the possible reasons would be that the major iron-rich mineral is goethite in IOF-B. It was report by the TWG (IMO 2013*f*) that surface area and water retention capacity increased with an increase in goethite content. Probably based on such a finding, it was stated in the individual schedule for "Iron Ore Fine" cargo that the IOF with goethite content ≥ 35% y mass may be shipped as an unliquefiable cargo (IMO 2010*b*). However, no evidence was given to clarify whether either the mineral goethite or the surface area governs water retention ability of IOF. It is unfortunate that goethite contents and surface areas for both IOFs could not be measured in this study; however, a literature survey was conducted. Mazeina and Novrotsky (2017) prepared several goethite samples with surface area of 60–270 m^2/g and hematite samples with surface area of 2–150 m^2/g, and it was found that retained amount of water by materials was linearly proportional to their surface area regardless of mineral types. Experimental data by Jurinak (1964) showed that the relationships between RH (20%–95%) and averaged water film thickness on material surface for goethite and hematite were similar. On the contrary, it was also found that the surface properties, such as entropy of water adsorption (Gast et al. 1974) and contact angle with water (Iveson et al. 2004) were different between goethite and hematite, which would affect water retention characteristics somewhat. It is not conclusive though it may be said that specific surface area would be more predominant, while goethite mineral may also affect water retention ability of IOF.

S–R_w relationship and compaction curves

Water retention characteristics of IOF-B in a full suction range is shown in Fig. 15 in terms of S–R_w and S–w relationships for loosest and densest specimens conducted in this study. It seems that the data points distribute in a "double S" shape (note the curves in Fig. 15 are not fitting curves, but hand-drawn lines), and the w corresponding to S_{th} is about w_{th} = 11%–13%. Compaction tests of IOF-B with different compaction energies were also conducted in this study as shown in Fig. 16. The tests with Proctor and modified Proctor energies were conducted following JIS (2009) standard A 1210, in which the size of mold and free fall height are slightly different from ASTM standards (ASTM 2003*b*, 2003*c*) resulting in slight differences of compaction energies (i.e., 550 and 2500 kJ/m^3 by JIS standard versus 600 and 2700 kJ/m^3 by ASTM standard, for Proctor and modified Proctor, respectively). For that the tests with MPFT energy, the compaction energy was applied in five layers by a 2.5 kg hammer with 25 blows per layer and 10 mm free fall height per blow.

Fig. 16. Compaction curves of IOF-B: (*a*) w versus ρ_d; (*b*) S_r–$(S_r)_{opt}$ versus ρ_d/ρ_{dmax}.

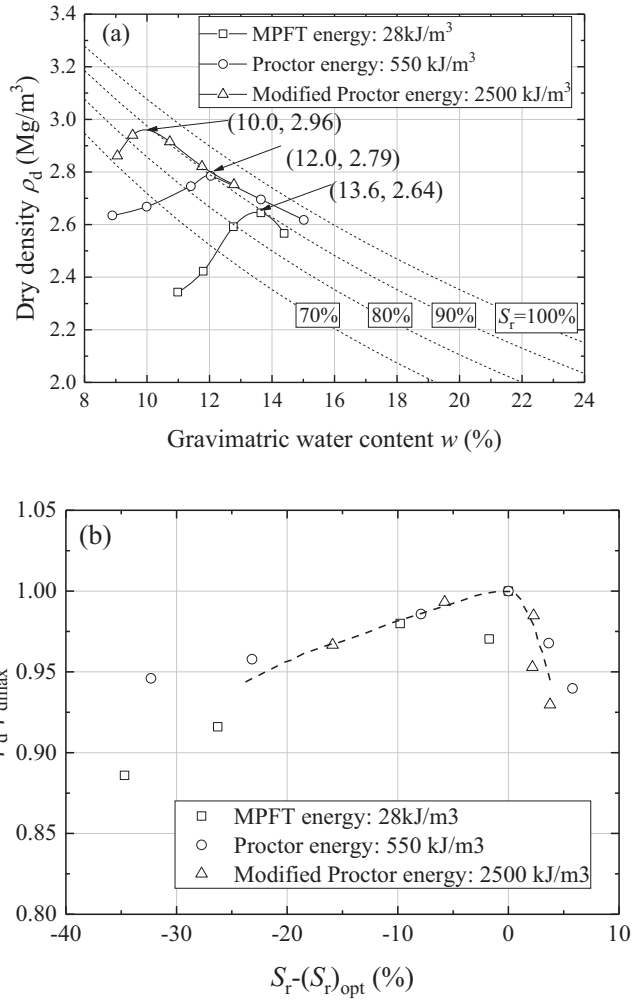

It can be seen from Fig. 16*a* that the optimum water content (w_{opt}) is in the range of 10.0%–13.6%, which is a similar range to that of w_{th}. Interestingly, from test data by Salager et al. (2010), similar results were also found (i.e., w_{opt} = 15% versus w_{th} = 13%∼15% for a clayey silty sand). On the contrary, Tatsuoka et al. (2016) proposed the concept of optimum degree of saturation $(S_r)_{opt}$, which was the corresponding S_r at point of (w_{opt}, ρ_{dmax}). They found, based on a large number of compaction data, that $(S_r)_{opt}$ rarely changed and the normalized relationship between S_r–$(S_r)_{opt}$ and ρ_d/ρ_{dmax} of the compaction test data converged to a very narrow zone for a material regardless of the compaction energy. It is found from Fig. 16*a* that $(S_r)_{opt}$ of IOF-B is about 90% and the S_r–$(S_r)_{opt}$ versus ρ_d/ρ_{dmax} relationship shown in Fig. 16*b* also follows the finding by Tatsuoka et al. (2016). From Figs. 15–16, it may be said that water of IOF-B at w_{opt} or $(S_r)_{opt}$ may be mostly retained by individual particles (i.e., V_{ws}). Apparently, according to assumptions in this paper, V_{ws} is retained firmer than V_{wv}. From this point of view, it is reasonable to say that compared with $(S_r)_{opt}$ of 90% for IOF-B and 90%–95% for other IOFs (IMO 2013*e*, 2013*f*), a TML equivalent to the water content of the intersection of MPFT and S_r = 80% line (see Fig. 1) keeps a safety margin of about 10%–15%.

Conclusions

As part of testing program for evaluation of liquefaction potential of the heap of IOF during the maritime transportation, the study presents results of water retention characteristics of two types of IOF. The following conclusions are obtained:

1. It is observed that water retention characteristic curves of a type of IOF (i.e., IOF-B) converge in terms of the S–w relationship for specimens with different e when S exceeds a threshold suction S_{th}. Based on this observation, it is proposed to divide pore water of unsaturated materials into water retained by individual particles V_{ws} and that retained by voids between particles V_{wv}.
2. It is revealed that water retention ability of tested IOF is higher than that of their references (i.e., artificial geomaterial mixtures) in the tested conditions. Furthermore, water retention ability of IOF-B seems to be higher than the other IOF (i.e., IOF-A) even in the suction range of 10^3–10^6 kPa. Based on a survey of the literature, effects of specific surface area and mineralogy may be possible reasons.
3. It is found that water content at the threshold suction (i.e., w_{th}) at water retention characteristic curves is close to optimum water content (w_{opt}) obtained by compaction tests for IOF-B. Given that the degree of saturation at peaks of compaction curves, $(S_r)_{opt}$, keeps relatively constant regardless of compaction energy, and it is of 90%–95% for IOF, it may be said that the proposed regulation for maritime transportation of IOF considers a safety margin of about 10%–15%.

Acknowledgements

The first author would like to express great gratitude to T. Sato at Integrated Geotechnology Institute Ltd., Japan, for his help in the experimental work, and H. Komine at Waseda University for his valuable comments on this work. The experimental work in this study was conducted at The University of Tokyo. This work was performed as a part of the activities of the first author at the Research Institute of Sustainable Future Society, Waseda Research Institute for Science and Engineering, Waseda University.

References

ASTM. 2003*a*. Standard classification of soils for engineering purposes (Unified Soil Classification System). ASTM standard D2487-00. American Society for Testing and Materials, West Conshohocken, Pa.

ASTM. 2003*b*. Standard test methods for laboratory compaction characteristics of soil using standard effort (12,400 ft-lbf/ft³ (600 kN-m/m³)). ASTM standard D698-00a. American Society for Testing and Materials, West Conshohocken, Pa.

ASTM. 2003*c*. Standard test methods for laboratory compaction characteristics of soil using modified effort (56,000 ft-lbf/ft³ (2,700 kN-m/m³)). ASTM standard D1557-00. American Society for Testing and Materials, West Conshohocken, Pa.

Birle, E., Heyer, D., and Vogt, N. 2008. Influence of the initial water content and dry density on the soil–water retention curve and the shrinkage behavior of a compacted clay. Acta Geotechnica, **3**(3): 191–200. doi:10.1007/s11440-008-0059-y.

Chen, X., Liu, M., and He, L. 2014. Shipwreck statistical analysis and suggestions for ships carrying liquefiable solid bulk cargoes in China. Procedia Engineering, **84**: 188–194. doi:10.1016/j.proeng.2014.10.425.

Delage, P., and Lefebvre, G. 1984. Study of the structure of a sensitive Champlain clay and of its evolution during consolidation. Canadian Geotechnical Journal, **21**(1): 21–35. doi:10.1139/t84-003.

Fredlund, D.G., Rahardjo, H., and Fredlund, M.D. 2012. Unsaturated soil mechanics in engineering practice. John Wiley and Sons, Inc., N.J.

Gallage, C.P.K., and Uchimura, T. 2010. Effects of dry density and grain size distribution on soil-water characteristic curves of sandy soils. Soils and Foundations, **50**(1): 161–172. doi:10.3208/sandf.50.161.

Gao, Y., and Sun, D. 2017. Soil-water retention behavior of compacted soil with different densities over a wide suction range and its prediction. Computers and Geotechnics, **91**: 17–26. doi:10.1016/j.compgeo.2017.06.016.

Gast, R.G., Landa, E.R., and Meyer, G.W. 1974. The interaction of water with goethite (α-FeOOH) and amorphous hydrated ferric oxide surfaces. Clays and Clay Minerals, **22**: 31–39. doi:10.1346/CCMN.1974.0220106.

Haynes, W.M. (*Editor*) 2010–2011. Handbook of chemistry and physics. 91st ed. CRC Press, Boca Raton, Fla. pp. 15-33–15-34.

Higuchi, T., Lu, L., and Kasai, E. 2017. Intra–particle water migration dynamics during iron ore granulation process. ISIJ International, **57**(8): 1384–1393. doi:10.2355/isijinternational.ISIJINT-2016-758.

Huang, S.-Y., Barbour, S.L., and Fredlund, D.G. 1998. Development and verifica-

tion of a coefficient of permeability function for a deformable unsaturated soil. Canadian Geotechnical Journal, **35**(3): 411–425. doi:10.1139/t98-010.

IMO. 2010*a*. Carriage of iron ore fines leading to marine casualties submitted by India. International Maritime Organization (IMO), MSC 87/INF.13.

IMO. 2010*b*. Carriage of iron ore fines that may liquefy. International Maritime Organization (IMO), DSC.1/Circ.63.

IMO. 2012. International Maritime Solid Bulk Cargoes (IMSBC) Code. International Maritime Organization (IMO).

IMO. 2013*a*. Early implementation of draft amendments to the IMSBC Code related to the carriage and testing of iron ore fines. International Maritime Organization (IMO), DSC.1/Circ.71.

IMO. 2013*b*. Report of the correspondence group on transport of iron ore fines in bulk (part 3). International Maritime Organization (IMO), DSC18/INF. 9.

IMO. 2013*c*. The Technical Working Group (TWG) report No. 1 "Terms of reference.1". International Maritime Organization (IMO), DSC18/INF. 10.

IMO. 2013*d*. The Technical Working Group (TWG) report No. 2 "Marine report". International Maritime Organization (IMO), DSC18/INF. 11.

IMO. 2013*e*. The Technical Working Group (TWG) report No. 3 "Iron ore fine Proctor–Fagerberg test". International Maritime Organization (IMO), DSC18/INF. 12.

IMO. 2013*f*. The Technical Working Group (TWG) report No. 4 "Reference tests". International Maritime Organization (IMO), DSC18/INF. 13.

IMO. 2013*g*. Research synopsis and recommendations by the Technical Working Group (TWG) report No. 5. International Maritime Organization (IMO), DSC18/6/14.

IMO. 2015. Amendments to the International Maritime Solid Bulk Cargoes (IMSBC) Code. International Maritime Organization (IMO), MSC.393 (95).

Iveson, S.M., Holt, S., and Biggs, S. 2004. Advancing contact angle of iron ores as a function of their hematite and goethite content: implications for pelletising and sintering. International Journal of Mineral processing, **74**: 281–287. doi:10.1016/j.minpro.2004.01.007.

JGS. 2009. Test method for water retentivity of soils. JGS standard 0151. Japanese Geotechnical Society.

JIS. 2009. Test method for soil compaction using a rammer. JIS standard A1210. Japanese Industrial Standard Committee.

Jurinak, J.J. 1964. Interaction of water with iron and titanium oxide surfaces: goethite, hematite, and anatase. Journal of Colloid Science, **19**: 477–487. doi:10.1016/0095-8522(64)90048-0.

Kawai, K., Karube, D., Ashida, W., and Kado, Y. 2000. Modeling of water retention curves with effects of void ratio. Doboku Gakkai Ronbunshu, **2000**(666): 291–302. doi:10.2208/jscej.2000.666_291. [In Japanese.]

Lins, Y., and Schanz, T. 2005. Determination of hydro-mechanical properties of sand. *In* Unsaturated soils: Experimental studies. Springer Proceedings in Physics. Vol. 93. *Edited by* T. Schanz. Springer, Berlin, Heidelberg. pp. 15–32. doi:10.1007/3-540-26736-0_2.

Mazeina, L., and Novrotsky, A. 2007. Enthalpy of water adsorption and surface enthalpy of goethite (α-FeOOH) and Hematite (α-Fe_2O_3). Chemistry of Materials, **19**: 825–833. doi:10.1021/cm0623817.

Nishimura, T., Koseki, J., Fredlund, D.G., and Rahardjo, H. 2012. Microporous membrane technology for measurement of soil-water characteristic curve. Geotechnical Testing Journal, **35**: 201–208. doi:10.1520/GTJ103670.

Ramanaidou, E.R., and Wells, M.A. 2014. Sedimentary hosted iron ores, treatise on geochemistry. 2nd ed. Elsevier Science.

Roberts, S.E., Pettit, S.J., and Marlow, P.B. 2013. Casualties and loss of life in bulk carriers from 1980 to 2010. Marine Policy, **42**: 223–235. doi:10.1016/j.marpol.2013.02.011.

Romero, E., Gens, A., and Lloret, A. 1999. Water permeability, water retention and microstructure of unsaturated compacted Boom clay. Engineering Geology, **52**: 117–127. doi:10.1016/S0013-7952(99)00067-8.

Salager, S., El Youssoufi, M.S., and Saix, C. 2010. Definition and experimental determination of a soil-water retention surface. Canadian Geotechnical Journal, **47**(6): 609–622. doi:10.1139/T09-123.

Tan Tian, J.U. 2019. Characterization of liquefaction and seepage properties under different saturation conditions of bauxite during maritime transport. Doctoral thesis, The University of Tokyo.

Tatsuoka, F., Fujishiro, K., Tateyama, K., Kawabe, S., and Kikuchi, Y. 2016. Properties of compacted soil as a function of dry density and the degree of saturation. Japanese Geotechnical Society Special Publication, **2**(4): 247–252. doi:10.3208/jgssp.JPN-099.

Wang, H., Koseki, J., and Nishimura, T. 2014. SWCC measurement of two types of iron ores. *In* Proceedings of the 6th International Conference on Unsaturated Soils, Unsat2014, Sydney. pp. 973–979.

Wang, H., Koseki, J., Sato, T., Chiaro, G., and Tan Tian, J. 2016*a*. Effect of saturation on liquefaction resistance of iron ore fines and two sandy soils. Soils and Foundations, **56**(4): 732–744. doi:10.1016/j.sandf.2016.07.013.

Wang, H., Koseki, J., Sato, T., and Miyashita, Y. 2016*b*. Geotechnical properties of a type of iron ore fines. Japanese Geotechnical Society Special Publication, **2**(14): 541–546. doi:10.3208/jgssp.JPN-079.

Wang, H., Sato, T., Koseki, J., Chiaro, G., and Tan Tian, J. 2016*c*. A system to measure volume change of unsaturated soils in undrained cyclic triaxial tests. Geotechnical Testing Journal, **39**(4): 532–542. doi:10.1520/GTJ20150125.

Wang, H., Koseki, J., and Cai., F. 2017*a*. Numerical evaluation of liquefaction potential of the heap of iron ore fines during maritime transportation. *In* Proceedings of the 19th International Conference of Soil Mechanism and geotechnical Engineering, Seoul, Korea, pp. 1447–1450.

Wang, H., Koseki, J., and Sato, T. 2017*b*. *p*-constant condition applied to undrained cyclic triaxial test of unsaturated soils. Geotechnical Testing Journal, **40**(4): 710–718. doi:10.1520/GTJ20160115.

Wang, H., Koseki, J., Nishimura, T., and Miyashita, Y. 2017*c*. Membrane filter properties and application of the filter to undrained cyclic triaxial test of unsaturated materials. Canadian Geotechnical Journal, **54**(8): 1196–1202. doi:10.1139/cgj-2016-0507.

Wang, H., Koseki, J., Cai, F., and Nishimura, T. 2018. Undrained monotonic triaxial loading behaviors of a type of iron ore fines. Canadian Geotechnical Journal, **55**(9): 1349–1357. doi:10.1139/cgj-2017-0480.

Wang, H., Koseki, J., and Nishimura, T. 2019. Permeability of saturated and unsaturated iron ore fines. Japanese Geotechnical Society Special Publication, **7**(2): 401–409. doi:10.3208/jgssp.v07.064.

Weber, W.J., and Morris, J.C. 1963. Kinetics of adsorption on carbon from solution. Journal of the Sanitary Engineering Division, ASCE, **89**(2): 31–60.

Young, J.F. 1967. Humidity control in the laboratory using salt solutions - A review. Journal of Applied Chemistry, **17**: 241–245. doi:10.1002/jctb.5010170901.